

# Blended Regenerative Anti-Lock Braking System and Electronic Wedge Brake Coordinate Control Ensuring Maximal Energy Recovery and Stability of All-Wheel-Motor-Drive Electric Vehicles

Mahmoud Said Jneid\*, Péter Harth

Automotive Technologies, Budapest University of Technology and Economics, Budapest, Hungary

Email: \*mah.jneid@edu.bme.hu

**How to cite this paper:** Said Jneid, M. and Harth, P. (2023) Blended Regenerative Anti-Lock Braking System and Electronic Wedge Brake Coordinate Control Ensuring Maximal Energy Recovery and Stability of All-Wheel-Motor-Drive Electric Vehicles. *Journal of Transportation Technologies*, 13, 465-495.

<https://doi.org/10.4236/jtts.2023.133022>

**Received:** May 29, 2023

**Accepted:** July 28, 2023

**Published:** July 31, 2023

Copyright © 2023 by author(s) and Scientific Research Publishing Inc.

This work is licensed under the Creative Commons Attribution-NonCommercial International License (CC BY-NC 4.0).

<http://creativecommons.org/licenses/by-nc/4.0/>



Open Access

## Abstract

ABS is an active safety system which showed a valuable contribution to vehicle safety and stability since it was first introduced. Recently, EVs with in-wheel-motors have drawn increasing attention owing to their greatest advantages. Wheels torques are precisely and swiftly controlled thanks to electric motors and their advanced driving techniques. In this paper, a regenerative-ABS control RABS is proposed for all-in-wheel-motors-drive EVs. The RABS is realized as a pure electronic braking system called brake-by-wire. A coordination strategy is suggested to control RABS compromising three layers. First, wheels slip control takes place, and braking torque is calculated in the higher layer. In the coordinate interlayer, torque is allocated between actuators ensuring maximal energy recovery and vehicle stability. While in the lower layer, actuator control is performed. The RABS effectiveness is validated on a 3-DOF EVSimulink model through two straight-line braking manoeuvres with low and high initial speeds of 50 km/h and 150 km/h, respectively. Both regular and emergency braking manoeuvres are considered with ABS enabled and disabled for comparison. Simulation results showed the high performance of the proposed RABS control in terms of vehicle stability, brake response, stopping distance, and battery re-charging.

## Keywords

EV Stability, Regenerative-ABS, Blended Braking, Energy Recovery, In-Wheel-Motor, Electronic-Wedge-Brake, Brake-by-Wire

## 1. Introduction

Braking is a safety-critical system that has a crucial effect on vehicle longitudinal and lateral behaviour. Besides the primary function of vehicle deceleration, the braking system impacts vehicle steering and stability, which becomes vital for stable manoeuvrability and handling. In conventional vehicles, hydraulic brake actuators are used to provide the brake service. The vehicle's kinetic energy is converted into heat by friction between the brake pad and wheel disc with frictional brakes.

Almost 25% of the vehicle's kinetic energy is lost through heat dissipation through braking activities [1]. However, at severe braking, the wheels' forces become greater than the road limit, leading to the wheels locking up and losing interaction with the road surface, which causes the vehicle to skid along and perhaps across the road. Meanwhile, the wheel's longitudinal force is minimum, and the vehicle no longer responds to further deceleration requests increasing the stopping distance considerably.

Losing the road-tire gripping affects not only the longitudinal dynamics but also the laterals. When the front wheels lock, vehicle steering is retarded and wheel forces become uncontrollable and the vehicle is said understeering behaviour. In contrast, the locking of the rear wheels leads to an undesired yaw motion where vehicle behaviour is oversteering [2]. These are the worst scenarios where vehicle stability and driver control are missed and subjected to a potential smash.

However, the recent developments and successful application of advanced chassis assistance active safety systems (ACAS), such as anti-lock braking system (ABS), electronic stability control (ESC), traction control (TC), and torque vectoring (TV) enabled promising answers for vehicle safety and stability [3] [4]. Nowadays, different ACASs can be introduced as one integrated control solution, which has become a crucial part of vehicle safety [5] [6]. ABS is one of the most effective ACAS solutions ever introduced due to its exceptional performance under all road conditions as active braking.

Recently ABS has been applied in almost all vehicle types due to its potential to address the challenges connected to vehicle stability, handling, and safety by preventing wheels from locking up, especially on slippery and  $\mu$ -split roads [7] [8]. These advantages put ABS ahead of the standardized safety systems list with the eighth highest priority [9]. The ABS constantly monitors and regulates wheels' acceleration within a given bandwidth by modulating cylinder pressure at each wheel [10] [11]. This way, wheel slip limits cannot be reached, maintaining maximum wheel-road grip the given friction coefficient  $\mu_{road}$  [12] [13] [14] [15]. ABS always guarantees maximum wheel-road gripping for different road types, significantly minimizing the brake distance. However, ABS improves not only the vehicle's longitudinal behaviour but also maintains lateral stability [16]. Vehicles equipped with ABS sustain high handling and stability at reduced stopping distance which cuts down their involvement in crashes [17]. For example,

the braking distance is reduced by more than 4% on roads with poor conditions with low and  $\mu$ -split [18]. Nevertheless, different studies showed higher reductions of up to 18% (4.33 m less compared with standard brakes) [19], or even up to 36% [9].

The ever-increasing concerns of climate change and claims to eliminate CO<sub>2</sub> emissions motivated automakers to devote massive efforts and take accelerated steps toward developing next-generation hybrid and pure EVs. Thus, the recent couple of years witnessed a continuous increment in on-road hybrid vehicles number as a pre-acknowledgement of the upcoming EVs. With the full adoption of EVs, CO<sub>2</sub> emissions can be ceased totally. The recent trends and advances in electrical drive technologies, namely electric motors (EMs), power electronics, and energy storage devices, suggest that EVs are shortly replacing internal combustion engine (ICE) vehicles [20] [21] [22].

Besides environmental protection, many other benefits are ensured by shifting to electrified mobility. Hybrid and EVs have a more straightforward drivetrain layout, fewer mechanical and hydraulic components, higher efficiency, improved fuel economy, electronic application of different ACASs, and realization of regenerative braking. Furthermore, EMs are the only power source, and their torque can be controlled over a wide speed range enabling seamless and efficient integration between different ACASs such as ABS and ESC [23] [24].

In hybrid and EVs, the vehicle's kinetic energy during braking can be converted into electrical energy via the regenerative braking system (RBS) [25] [26]. RBS provides an intelligent solution as a pure electronic brake, also called brake-by-wire (BBW), owing to the absence of a direct connection with the brake pedal. EMs work as generators at braking periods delivering electric energy back to the battery pack via devoted power electronics.

Amongst all advantages, energy recovery is the most promising answer to the main challenges yet hinders EV mass production. Such hurdles include cost, range, charging time, and battery lifespan. For example, during normal driving, regenerative braking allows for more than 37% of the kinetic energy to be recovered [19]. However, the amount varies massively depending on the driver's behaviour and the driving path. In other words, the deceleration rate in urban is high; thus, a considerable amount of energy can be recovered, improving fuel consumption and extending the vehicle range [27]. For instance, the EVs range is extended up to 15% [28], and the fuel consumption is decreased between 10% - 25% in hybrid vehicles [29].

Nevertheless, the recovered energy is hindered by two main factors, the battery state of charge (SOC) and the vehicle speed. At high SOC (80% - 95%), the battery management system (BMS) ceases charging for safety and durability reasons such as battery lifespan, temperature, and mechanical structure [21] [30]. Thus, the motor electromotive force (EMF) is below the regeneration limits at lower speeds. Additionally, energy recovery is limited by the motor/generator max power and the battery charging rate. If the battery SOC and motor speed limits are not reached, regenerative torque can be still developed but might lack

the vehicle deceleration requirements. However, for safety issues, the braking system must be reliable and always available under any conditions and respond to brake requests from the driver or even other ACASs like ESC. Due to the unavailability of RBS in some cases, it must be boosted by another sustainable braking system.

Currently, hybrid and pure EVs are equipped with a hydraulic ABS besides the RBS realizing combined brakes [31] [32]. However, ABS functions and RBS cannot be set off at the same time where always a trade-off between safety and energy recovery must be committed [33] [34] [35]. For example, ABS is not triggered when the brake request is within the RBS capacity as long as the battery can be recharged via RBS for significantly maximum energy recuperating. The absence of ABS is undesired in this case, especially at high-speed and severe braking, where ABS becomes indispensable. Nonetheless, compromising the hydraulic ABS adds extra cost and complexity to the control system and vehicle structure. Thus, this combination does not realize a fully integrated BBW system required for next-generation EVs.

Besides, the wheel slip constantly changes around a critical slip value due to logic control used in standard on-off acceleration-based ABS; hence, the average longitudinal force is lower than the maximum available limit. Also, this undesired oscillation creates uncomfortable vibration on the brake pedal and affects the total performance [36]. Though, the low control frequency of solenoid valves, lacks the response in transient dynamic leading to a significant delay and limitation in the ABS functionality [16].

For the previous issues, this article looks to use in-wheel-motors (IWMs) as RBS and replace conventional hydraulic actuators with electronic ones, namely electronic wedge brakes (EWB). Thus IWMs and EWBs work together to realize a pure BBW system with multi-actuators. With this arrangement, ABS features and their advantages can be implemented based on an electronic version thanks to precise control of IWMs and EWBs, providing a wide range of continuous braking torque [37] [38]. The integration between IWMs and EWBs results in a multi-actuator system requiring a braking strategy to coordinate and control individual actuators.

Coordinate control is responsible for command distribution between different systems and activation of the suitable actuators [39]. Generally, coordinate controllers of integrated RBS consist of three layers, the higher layer for target parameters tracking, the interlayer for reference coordination, and the lower layer for actuators operation control [40] [41]. Across the three layers, different types of controllers have been widely used, such as classical proportional-integral-derivative (PID), optimal theory using linear quadrature regulator (LQR), nonlinear backstepping control, robust sliding mode control (SMC), adaptive gain scheduling (AGS), model predictive control (MPC), and intelligent fuzzy logic (FL) and neural networks (NN) [11] [42]. In integrated RBS, the control strategy can be optimized for either maximal energy recuperation or vehicle stability and safety.

In literature, several approaches are mainly explored. Chen (2021) proposed a cooperative control with three layers to coordinate the operation of ABS and electromechanical energy recovery BBW system [13]. Subramaniyam (2021) presented an integrated regenerative and pneumatic braking system based on wheel slip control using SMC and responsive regenerative braking for an electrified vehicle [43]. Tang (2022) introduced a coordinated MPC strategy of a compound regenerative and hydraulic ABS for an all-wheel-drive (AWD) battery EV with two central motors [44]. Zhao (2019) provided a cooperative control strategy for maximal energy recovery while regulating wheel slip by devoting front wheels for regenerative braking and rear wheels for frictional braking [45]. Mei (2021) proposed an adaptive fuzzy SMC for optimal wheel slip-based RBS with maximum energy recovery and braking stability [46]. Vodovozov (2021) presented a neural network-based blended braking allocation controller that guarantees maximum energy recovery using torque gradient control independent of the tire model [47]. Torinsson (2020) suggested an energy-efficient-based control allocation algorithm to distribute braking torque demand on the four EMs during deceleration [48]. Heydrich (2021) announced a blended regenerative and frictional BBW control for EVs with IWMs. The ABS feature was realized by implementing a wheel slip control based on the integral SMC method [49]. De Castro (2012) presented an integrated regenerative and frictional ABS control for EVs with IWMs. The control includes an adaptive robust wheel slip control layer and a torque allocator layer triggered by the brake supervisory layer [50]. Han (2014) proposed hierarchical cooperative regenerative braking control based on optimum brake torque allocation for maximal energy recovery and lateral stability sustainability of a front axle drive HEV. The control system comprises a higher-level part dedicated to LQR-based direct yaw rate control and a lower-level part devoted to brake torque allocation using adaptable weighing factors [51].

This paper considers blended RABS and EWB coordinate control to ensure maximal energy recovery while maintaining the safety and stability of all-IWMs-drive EVs. The control structure compromises an upper monitoring layer where wheels slip control takes place, a coordination interlayer, and a lower layer where IWMs and EWBs actuators are controlled. The remainder of the paper is structured as follows. Section 2 presents systems models. Section 3 introduces different RBSs. Section 4 illustrates the main principles of wheel anti-locking under ABS. Section 5 highlights the proposed blended RABS and EWB coordinate control design. Section 6 reveals and discusses the results, followed by Section 7, concluding the work.

## 2. Systems Models

The all-IWMs-drive EV structure is suggested to compromise the followings: four e-unit (4xIWMs, power electronics, and 4xEWBs), battery pack, acceleration (braking) pedal, electronic control unit (ECU), and vehicle dynamic model (VDM). **Figure 1** shows a schematic representation of the proposed structure.

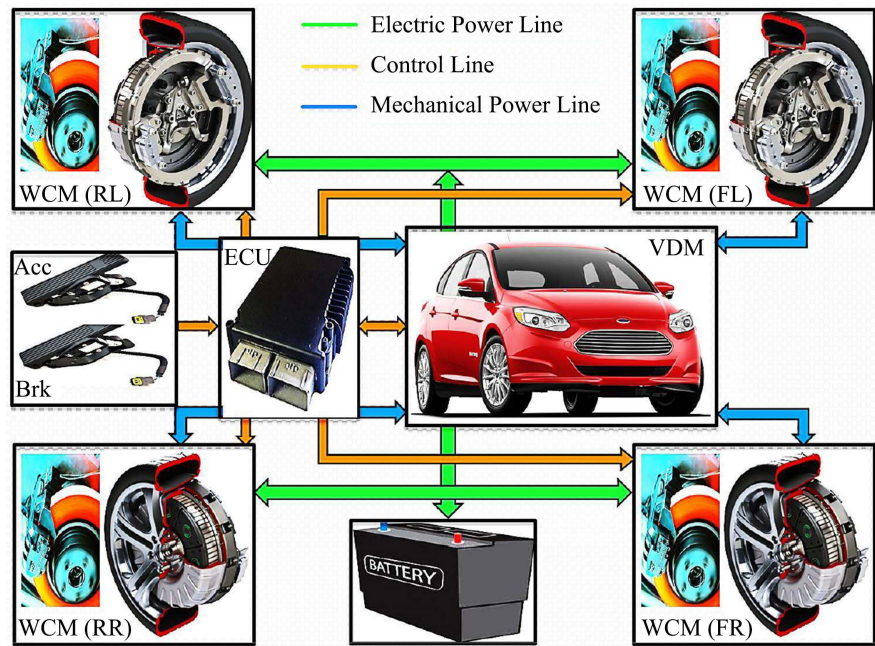


**Figure 1.** Schematic representation of the EV structure for the proposed RABS.

### 2.1. Vehicle Dynamic Model

The VDM plays an essential role in studying and analysing the braking system and other ACAS. Since this work considers only normal and emergency straight-line braking, a 3-DOFs EV model provides sufficient information on vehicle motion and brake dynamics for RABS validation. **Figure 2** shows a schematic diagram of the VDM describing longitudinal, lateral, and yaw motions with wheel rotations. However, the suspension in this model is considered rigid where pitch and roll motions are neglected, and only the front wheels can be steered. The equations of motion are given as follows [52]:

$$m(\dot{V}_x - \gamma V_y) = (F_{fl}^x + F_{fr}^x) \cos \delta_f - (F_{fl}^y + F_{fr}^y) \sin \delta_f + (F_{rl}^x + F_{rr}^x) \quad (1)$$

$$m(\dot{V}_y + \gamma V_x) = (F_{fl}^y + F_{fr}^y) \cos \delta_f + (F_{fl}^x + F_{fr}^x) \sin \delta_f + (F_{rl}^y + F_{rr}^y) - m\gamma V_x \quad (2)$$

$$I_z \dot{\gamma} = l_f (F_{fl}^y + F_{fr}^y) \cos \delta_f + l_f (F_{fl}^x + F_{fr}^x) \sin \delta_f - l_r (F_{rl}^y + F_{rr}^y) + M_z \quad (3)$$

$$M_z = \frac{T_f}{2} [(F_{fl}^x + F_{fr}^x) \cos \delta_f + (F_{fl}^y - F_{fr}^y) \sin \delta_f] - \frac{T_r}{2} (F_{rl}^x - F_{rr}^x) \quad (4)$$

where:  $m$  denotes vehicle total mass,  $\dot{V}_x$  ( $V_x$ ) vehicle CG longitudinal acceleration (velocity),  $\dot{V}_y$  ( $V_y$ ) vehicle CG lateral acceleration (velocity),  $\dot{\gamma}$  ( $\gamma$ ) vehicle CG yaw rate (angle),  $I_z$  vehicle yaw moment of inertia,  $\delta_f$  front wheels steering angle,  $F_i^x$  ( $F_i^y$ ) wheel  $i$ -th longitudinal (lateral) force,  $M_z$  wheels yaw moment,  $l_f$  ( $l_r$ ) CG distance from the front (rear) axle. Subscripts  $fl$  ( $fr$ ) and  $rl$  ( $rr$ ) indicate the front-left (right) and rear-left (right) wheels, respectively,  $T_f$  ( $T_r$ ) represents the track width of the front (rear) wheels.

Finally, the vehicle sideslip angle  $\beta$  is defined as the angle between the vehicle's longitudinal axis and the direction of its travel concerning the CG.

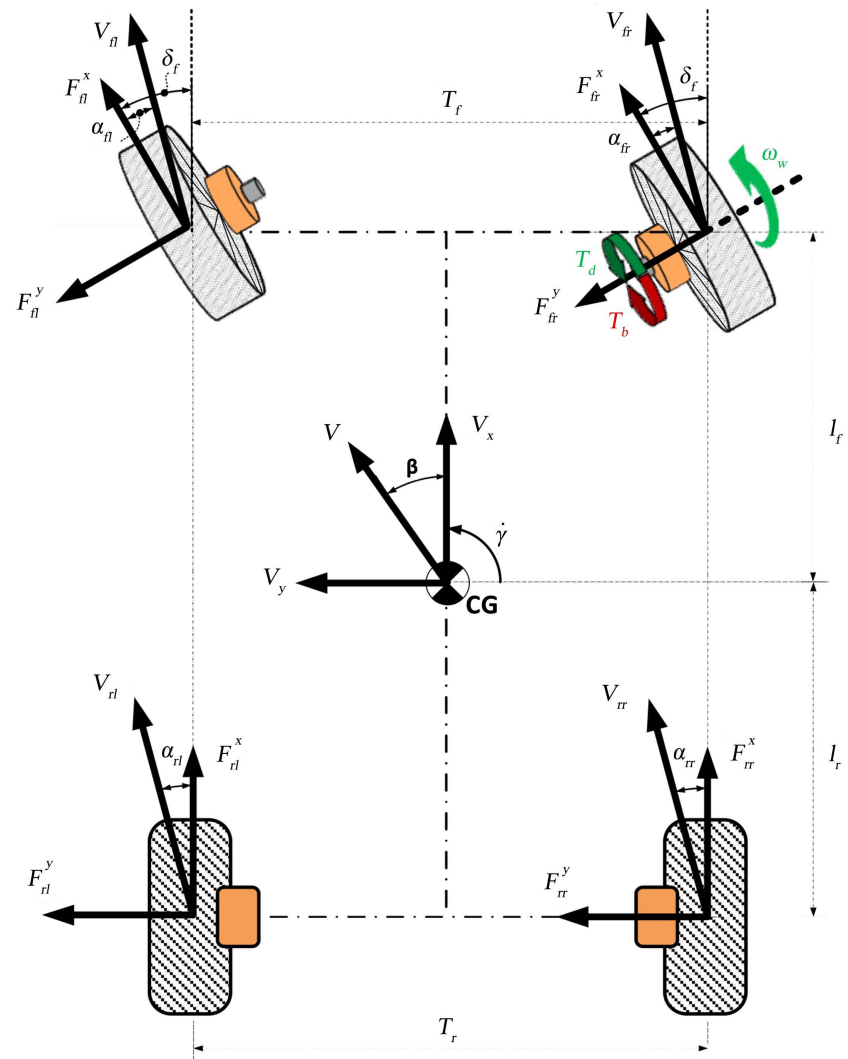


**Figure 2.** Schematic representation of VDM with 3-DOF and wheels rotation.

$$\beta = \tan^{-1} \frac{V_y}{V_x} \quad (5)$$

## 2.2. Tire Model

The wheels are the only elements in direct contact with the ground and considerably influence the vehicle's behaviour. Therefore, the tire model should provide accurate longitudinal and lateral dynamics calculations. Various tire models have been widely investigated in the literature, e.g., the magic formula (MF) and the brush model. This work considers a nonlinear MF model due to its simplicity and low calculation requirements. The model uses empirical parameters to describe the tire-road interaction at the contact point. Braking and cornering forces are calculated as functions of slip ratio  $\kappa$  and slip angle  $\alpha$ . Empirical parameters can be specified based on the wheels' vertical loads and camber angle. The equation describing the MF tire is given as follows [53]:

$$y = D \sin \left[ C \arctan \left\{ Bx - E \left( Bx - \arctan ( Bx ) \right) \right\} \right] \quad (6)$$

To make the model output curve symmetric concerning the coordinate origin, horizontal and vertical displacements are defined as follows [53]:

$$Y = y + S_v \quad (7)$$

$$x = X + S_h \quad (8)$$

where:  $y$  is the model output  $(F_x, F_y)$ ,  $Y$  is the model output after vertical displacement  $S_v$ ,  $x$  is the model input ( $\kappa$  or  $\alpha$ ), and  $X$  is the input with a horizontal displacement  $S_h$ .  $B$ ,  $C$ ,  $D$ , and  $E$  are the stiffness, the shape, the peak, and the curvature coefficients, respectively. The tire behaviour depends on these coefficients, and they vary from one road to another [28]. The wheels slip ratio (driving/braking) is given as follows:

$$\kappa = -\frac{v_x - r\omega_w}{v_x} \quad (9)$$

The tires slip angle  $\alpha_f/\alpha_r$  can be calculated based on geometric derivation using wheel velocity vectors as follows [54]:

$$\alpha_{fl} = -\delta_f + \tan^{-1} \left( \frac{v_y + Yl_f}{v_x - Y\frac{T_f}{2}} \right) \quad (10)$$

$$\alpha_{fr} = -\delta_f + \tan^{-1} \left( \frac{v_y + Yl_f}{v_x + Y\frac{T_f}{2}} \right) \quad (11)$$

$$\alpha_{rl} = \tan^{-1} \left( \frac{v_y - Yr}{v_x - Y\frac{T_r}{2}} \right) \quad (12)$$

$$\alpha_{rr} = \tan^{-1} \left( \frac{v_y - Yl_r}{v_x + Y\frac{T_r}{2}} \right) \quad (13)$$

The rotational dynamics for each wheel is the sum of driving, braking, and wheel-road torques acting around the wheel's spin axis, as shown in **Figure 2**. The wheel rotational behaviour can be expressed according to the following torque balance equation [55]:

$$I_w \dot{\omega}_w = T_d - T_b - rF_x \quad (14)$$

where:  $v_x$  ( $v_y$ ) is the vehicle longitudinal (lateral) velocity,  $I_w$  denotes the wheel inertia,  $\dot{\omega}_w$  is the wheel angular velocity derivative,  $T_d$  is the driving torque,  $T_b$  is the wheel braking torque, and  $r$  is the wheel's effective radius.

Vertical load at each wheel, taking into account the load transfer due to the longitudinal and lateral accelerations, can be calculated as follows [56]:

$$F_{fl}^x = \frac{gml_r}{2(l_r + l_f)} - \frac{m\dot{V}_x h_{cg}}{2(l_r + l_f)} - \frac{m\dot{V}_y h_{cg}}{2(l_r + l_f)T_f} \quad (15)$$

$$F_{fr}^x = \frac{gml_r}{2(l_r + l_f)} - \frac{m\dot{V}_x h_{cg}}{2(l_r + l_f)} + \frac{m\dot{V}_y h_{cg}}{2(l_r + l_f)T_f} \quad (16)$$

$$F_{rl}^x = \frac{gml_r}{2(l_r + l_f)} + \frac{m\dot{V}_x h_{cg}}{2(l_r + l_f)} - \frac{m\dot{V}_y h_{cg}}{2(l_r + l_f)T_r} \quad (17)$$

$$F_{rr}^x = \frac{gml_r}{2(l_r + l_f)} + \frac{m\dot{V}_x h_{cg}}{2(l_r + l_f)} + \frac{m\dot{V}_y h_{cg}}{2(l_r + l_f)T_r} \quad (18)$$

### 3. Regenerative Braking System

In hybrid and EVs, RBS converts the vehicle's kinetic energy during braking into electrical energy stored in the battery pack instead of being dissipated as heat in conventional frictional braking [26] [44]. RBS uses EMs as generators during braking to harness the vehicle's kinetic energy as electrical energy [44]. In literature, almost all RBS are realized on essential dynamic braking, which uses the traction battery to absorb the generated energy [28]. The recovered energy can effectively extend the range of EVs and reduce fuel consumption and emissions in hybrid vehicles. The level of fuel consumption improvement (reduced by 8% - 25%) depends on the driving path and behaviour [29] [57] [58].

#### 3.1. The Integrated Regenerative and Frictional Braking System

Generally, regenerative torque is insufficient to brake the vehicle under specific conditions [16]. Also, RBS cannot be activated in various situations, for example, when the battery SOC is high, or the vehicle speed is below the limit of torque production. With these considerations, using a ceaseless frictional braking system (FBS) with RBS is expected to cover the remaining torque. The integration between FBS and RBS is essential and requires a braking strategy to control both [59]. Depending on the integration strategy, the resulting brakes can be classified into two types: a blended RBS (also series or superimposed) and a cooperative RBS (also parallel or non-blended) [29]. The integrated braking system has three main modes of operation: pure regenerative braking, pure frictional braking, and blended regenerative-frictional braking.

#### 3.2. The Integrated Regenerative and Frictional Braking System

Both RBS and FBS always work simultaneously in cooperative braking, as shown in **Figure 3(a)**. The brake command is distributed between the two systems based on a constant ratio [58]. The FBS is permanently connected to the brake pedal and boosted all the time by RBS [29]. The driver's experience with the amount of brake pedal depressing and travel must remain similar to in conventional brake. This can be achieved by adjusting the brake pressure produced at a given pedal's input. Thus, RBS can only contribute to a limited braking torque

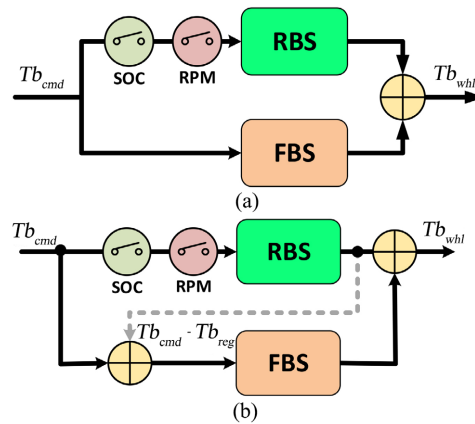


**Figure 3.** Schematic representation of the (a): cooperative RBS and (b): blended RBS.

[58]. However, cooperative braking has the advantages of simple control and high reliability owing to maintaining the hydraulic brake structure unchanged, providing the total braking torque alone when RBS is deactivated.

### 3.3. The Integrated Regenerative and Frictional Braking System

Blended braking is based on proper blending between RBS and FBS brake torques [29] [47]. When the demand is within EMs capacity, only RBS operates to meet this demand [47] [58]. However, if the brake demand is higher than the RBS torque capacity, FBS provides the remaining portion that is not covered by RBS [58]. In this strategy, the braking priority is maintained by RBS, where EMs operate at max power providing a significant braking torque [60]. The brake control must ensure that the vehicle's deceleration is independent of its speed for pedal input [58].

RBS takes precedence over FBS, especially at slow braking or low deceleration. When the brake pedal is depressed too fast (hard), the brake control provides more braking torque through the FBS for faster deceleration. Here, the brake pedal is separated from the friction brake callipers, enabling real electronic brakes, also called BBW. Control of blended braking is more complex but demonstrates improved performance and higher energy recovery than the cooperative system [45]. **Figure 3(b)** shows a schematic representation of the blended RBS.

## 4. Wheels Anti-Locking Main Principals under ABS

The basic concept of the conventional ABS relies on regulating wheels' acceleration around a value of the maximum  $\mu_{road}$  is maintained [61]. Fortunately, for all road types,  $\mu_{road}$  is max within a specific range of wheel slip ratio, also called ABS active zone. If the wheel slip is controlled through this range, stable wheel performance is guaranteed, and maximum gripping is obtained [62]. There are two main techniques to prevent wheel locking under ABS: a standard hydraulic acceleration-based (also on-off, logic, or discontinuous) and electronic slip-based (also BBW, non-logic, regenerative, or continuous) [8] [9] [18].

#### 4.1. Hydraulic Acceleration-Based ABS

In acceleration-based, the wheel slip is controlled by monitoring and maintaining the wheel acceleration within a given window. The acceleration is estimated using the wheel angular velocity measurement and used as control feedback. The ECU continuously reads wheel speed sensor information to calculate the vehicle speed and wheel slip ratio and sends control signals to the hydraulic brake actuators. Hydraulic actuators are switched on and off based on ECU control signals to reduce, maintain, or increase pressure, ensuring the wheel slip ratio is always within the ABS stable range (10% - 30%). Thus wheels never lock up, and maximum force transfer is realized [62] [63]. Below this range, the wheel behaviour tends to be more slippery (whole spinning at  $\kappa = 0\%$ ), and above this range, it tends to be more skidding (full skidding at  $\kappa = 100\%$ ). ECU switches between the three modes continuously when ABS is enabled [6]. However, with the on-off operation of the actuators, undesired vibrations appear on the pedal, which makes an uncomfortable feeling for the driver, and the brake performance is considerably decreased [19].

#### 4.2. Electronic Slip-Based ABS

ABS can also be implemented electronically based on wheel slip, where wheel slip is directly controlled by a non-logic control method. Fortunately, monitoring and controlling wheel slip instead of acceleration in the hydraulic ABS allow for realizing a slip-based ABS, also regenerative ABS (hereafter referred to as RABS). Wheel slip is more efficient in controlling brake force and eliminating the vibration on the brake pedal [7]. The continuous slip regulation can be achieved via RBS, where EMs produce constant braking torque. The slip ratio target at which the force transfer is maintained maximum is in the range of 10% - 20% [64] [65]. RABS highly fits the layout and packaging requirements of future EVs. However, RABS must be robust enough, comparable to acceleration-based ABS, to handle the uncertainties generated by the rapid changes in the road surface [43].

### 5. The Proposed Blended RABS and EWB Coordinate Control

Implementing ABS features utilizing IWMs and EWBs allows for obtaining an integrated RABS. For precise brake torque control of each system, the controller must be designed carefully. However, IWM and EWB actuators should intervene and leave seamlessly, providing continuous braking torque and a similar feeling to conventional brakes. The operation modes of the integrated brakes can be set based on specific rules. For example, when the wheel slip ratio is below 10% a blended braking, between 10% - 20% pure regenerative braking, and above 20% pure frictional braking [32]. In this work, a blended RABS and EWB coordinate control strategy is proposed ensuring maximal energy recovery while maintaining the stability of all-IWMs-drive EVs. As shown in **Figure 4**, the suggested RABS control comprises three control layers: the high-level layer, the coordinate

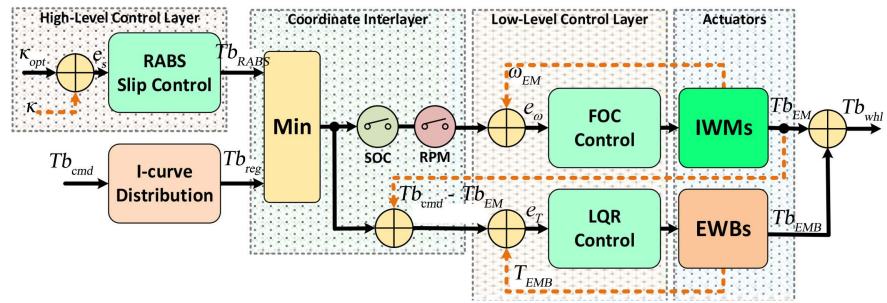


**Figure 4.** Schematic representation of the proposed blended RABS coordinate control.

interlayer, and the low-level layer. In the higher layer, a wheel slip control and brake torque ideal distribution takes place. In the interlayer, brake torque coordination between the IWMs and EWBs is present, while brake actuators control comes up in the low layer. The following subsections describe each layer in more detail.

### 5.1. Ideal Distribution of Brake Torque (I-Curve)

The function of the braking system is to decelerate the vehicle quickly and safely while maintaining its direction under control. During the braking, the vehicle load is shifted between the front and rear axles resulting in an unbalanced distribution of the braking forces, and the stopping distance is considerably increased [66]. A correct distribution of braking torques between the front and rear axles and left and right wheels have a crucial impact on brake performance and vehicle behaviour. The front-to-rear distribution should be calculated from a vehicle stability standpoint, considering that rear wheels must never lock up before the front ones [50]. Maximum braking efficiency corresponding to the shortest stopping distance is obtained through employing correct distribution strategies of braking torques, e.g. wheels load [58]. An effective distribution method widely used is based on the ideal-curve distribution between front and rear axles. Braking with a ratio below the curve means most braking is provided by the front axle, while values above the curve cause a significant contribution by the rear axle [58] [66]. The brake force required for a constant vehicle deceleration is given in the following equation:

$$F_b = m_v \alpha_x (g) = F_{bf} + F_{br} \tag{19}$$

The coefficient of proportionality of the ideal allocation between the front and rear axle is given by the wheels' vertical loads ratio:

$$P = F_{bf} / F_{br} = F_{zf} / F_{zr} \tag{20}$$

Thus, the ideal braking force portion of the front and rear axles can be calculated in terms of the wheels' vertical loads proportionality as follows:

$$F_{bf} = P m_v \alpha_x / (1 + P) = P F_b / (1 + P) \tag{21}$$

$$F_{br} = m_v \alpha_x / (1 + P) = F_b / (1 + P) \tag{22}$$

where:  $F_b$  is the total braking force for a given vehicle deceleration,  $F_{bf}$  ( $F_{br}$ )

the ideal front (rear) axle braking force.  $P$  front and rear axles brake force ratio based on I-curve distribution.

## 5.2. Wheels Slip Control (the Higher Layer)

For RABS based on wheel slip control feasibility, a relationship between IWMs torques and the wheel slip must exist. This relationship can be obtained by working out the time derivative of the wheel slip ratio and further fixing it according to:

$$Tb_{cmd} = \left( \frac{J_{w(\kappa+1)}}{L_r m / (L_f + L_r)} + r \right) F_x - \frac{J_w}{r} (V_x \dot{\kappa}) \quad (23)$$

## 5.3. The Brake Coordination Strategy (the Interlayer)

The braking torque reference obtained from the wheel slip control is compared with the driver's brake request to realize vehicle deceleration in response to the driver's command. Coordinate control is responsible for braking torque distribution between the IWMs and EWBs based on the blended braking method. The torque distribution unit continuously reads the braking torque required and compares it with the IWMs speed-torque map to determine the brake torque portion that IWMs can provide. Then the confined reference is weighted by the vehicle speed and the battery SOC limiting factors, having a value between 0 - 1. The IWMs torque is estimated and subtracted from the total brake torque demand at each wheel to calculate the torque portion of EWBs. EWBs intervene and deliver the appropriate braking torque part, which IWMs cannot cover (e.g., working in constant power area or flux weakening mode) to meet the driver's demand (800 Nm), as shown in **Figure 5**. Thus there are three operation modes defined by torque allocation control as follows:

- Pure regenerative braking: when the total brake torque demand is within the IWMs power capacity, given that the battery SOC and the vehicle speed allow for energy recovery, IWMs are only used to generate a pure regenerative torque, and the energy recovery is maximum.

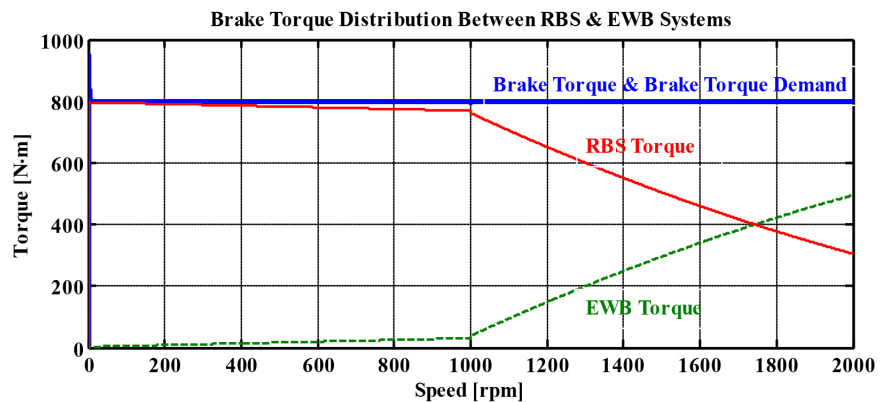


**Figure 5.** Blended regenerative and frictional torques generated by IWMs and EWBs.

- Blended regenerative-frictional braking: when the required braking torque is out of the IWMs power capacity, given that the SOC and vehicle speed factors allow for energy recovery, then both IWMS and EWBs work and generate a mixed brake torque, and the energy recuperation is SOC-dependent.
- Pure frictional braking: when the required braking torque is within (out) the power capacity of IWMs, given that the SOC state and (or) the vehicle speed does not allow any energy recovery, then EWBs are only used to generate a pure frictional torque, and the energy recovery is zero.

## 6. Simulation Results and Discussion

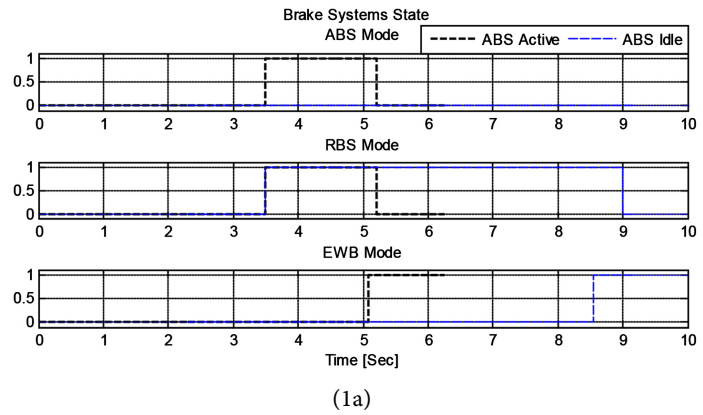
The performance of the proposed RABS is evaluated through simulation brake tests done on a 3-DOF vehicle model with 4xIWMs and 4xEWBs in MATLAB/Simulink. In this simulation, the battery pack is modelled as four individual packs for each wheel unit, allowing a high level of modularity. Two straight-line braking manoeuvres were performed, the low speed (50 km/h) and the high speed (150 km/h). Results are demonstrated and compared regarding vehicle speed, wheel speed, wheel torque, wheel slip ratio, and battery SOC. A thick line emphasizes responses for ABS enabled and a thin line for ABS disabled.

### 6.1. The Low-Speed Braking Manoeuvre

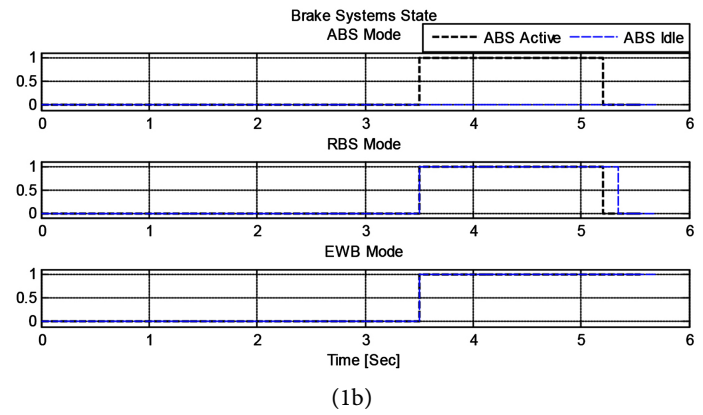
In this manoeuvre, two braking scenarios are carried out, a regular emergency braking with brakes partially and fully applied, respectively.

- Regular braking Scenario (1A)

**Figure 6(1a)** shows the working areas of both IWMs and EWBs to meet the torque demand under braking manoeuvre 1A with ABS enabled/disabled. It can be seen that the ABS activation period starts with brake application at 3.5 s and lasts until the vehicle speed becomes less than 7 km/h at 5.2 s, where ABS is disabled by the control system automatically. When ABS is enabled, the RABS control switches between modes: firstly from pure regenerative braking (3.5 s - 5.06 s), then blended braking (5.06 s - 5.2 s), and lastly, pure frictional braking (5.2 s to 6.25 s) at which vehicle comes to a standstill. Similarly, when ABS is disabled (over the whole brake period), the RABS control switches between modes: initially from pure regenerative (3.5 s to 8.6 s), then blended (8.6 s - 9 s), and finally to pure frictional (9 s - 10 s) until vehicle's full stop. **Figure 7(1a)** shows the vehicle speed and the front-right wheel speed. It can be noted that the time required to reach a vehicle's complete halt is relatively short (2.75 s) with ABS enabled, while it takes almost two times the previous period (6.5 s) with ABS disabled. In other words, the stopping distance with ABS is much shorter. **Figure 8(1a)** shows the regenerative and frictional torques of the front-right wheel with both ABS enabled/disabled. When ABS is active, the IWM works at the highest performance, providing maximum pure regenerative torque (-800 Nm), which swiftly brakes the vehicle. EWB intervened only for a brief period at the end of the braking and provided a small braking torque. When ABS is idle, the

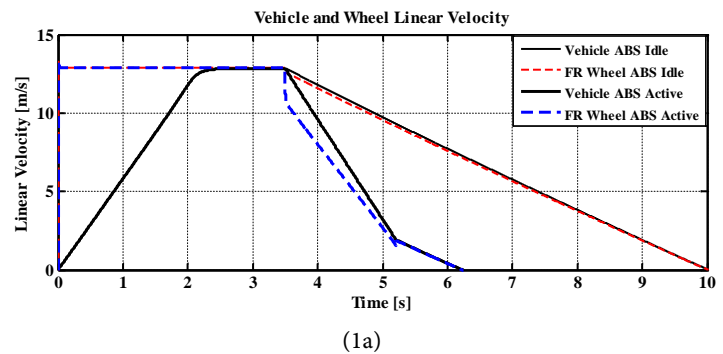


(1a)

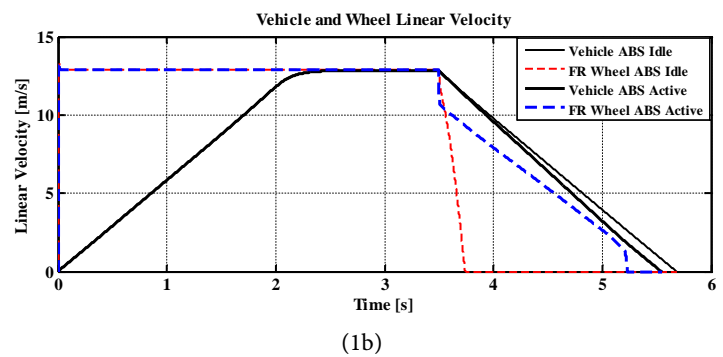


(1b)

**Figure 6.** ABS status and activation periods of IWMs and EWBs in the low-speed manoeuvre.



(1a)



(1b)

**Figure 7.** Vehicle and front-wheel speeds with ABS enabled/disabled in the low-speed manoeuvre.

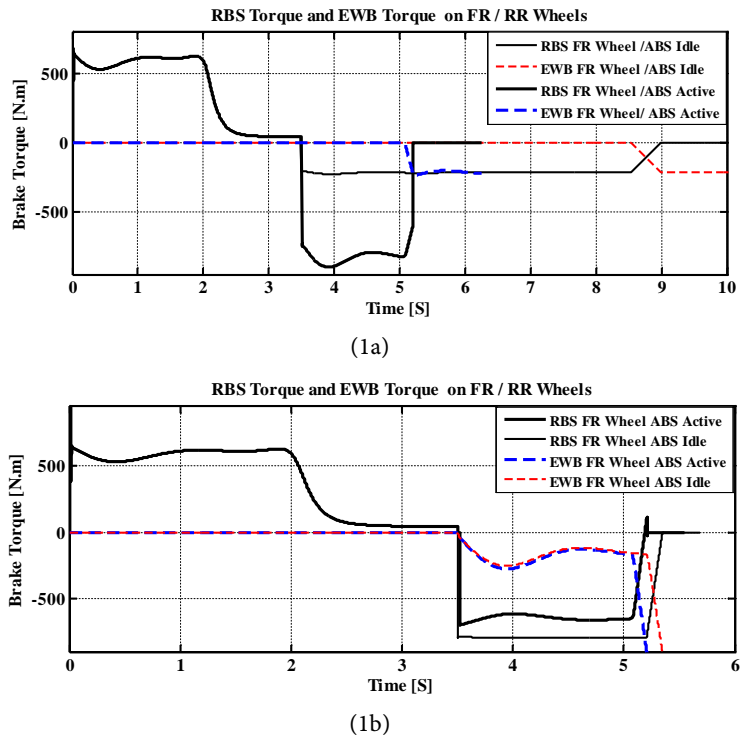
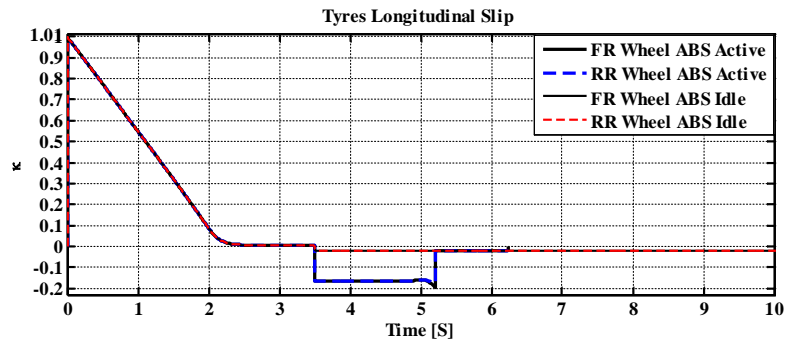


**Figure 8.** IWM and EWB torques of the front-right wheel with ABS enabled/disabled in the low-speed manoeuvre.

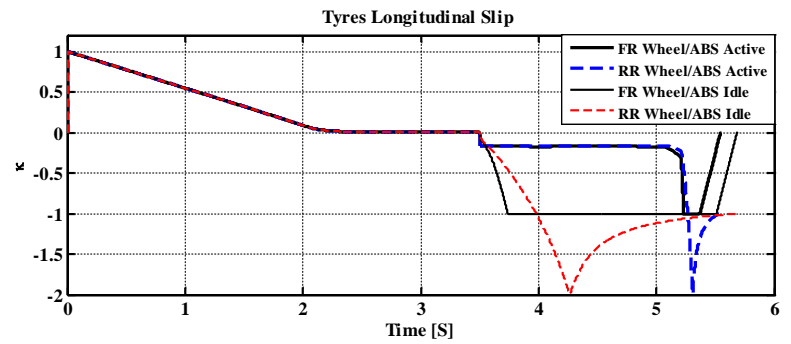
IWM generates a constant regenerative torque ( $-200$  Nm) much lower than that with ABS active, increasing the stopping distance significantly. Similarly, EWB starts at the end of braking, providing a small portion (blended torque) which increases until the point IWM quits, while EWB keeps working alone, generating pure frictional torque ( $-200$  Nm) until the vehicle comes to a full stop. **Figure 9(1a)** shows the slip ratio of the front (rear)-right wheels with both ABS enabled/disabled. It is noted that with ABS, the slip ratio is regulated at an optimum value of  $\kappa \approx 0.18$ , at which maximum  $\mu_{road}$  is maintained, allowing a maximum gripping force. **Figure 10(1a)** shows the brake forces generated by the front (rear)-right wheels with different ratios due to ideal distribution. **Figure 11(1a)** shows the SOC for battery packs BP1 and BP3 when ABS is enabled/disabled. It is evident that when ABS is enabled, the energy recovery is much higher than when ABS is disabled, and battery packs are recharged faster in this case.

- Emergency braking Scenario (1B)

**Figure 6(1b)** shows the working areas of both IWMs and EWBs to meet the braking demand in emergency braking manoeuvres with ABS enabled/disabled. The ABS is enabled on the brake pedal, hitting at 3.5 s until the vehicle decelerates to a speed below 7 km/h at 5.2 s. ABS is automatically disabled, and standard frictional braking begins until the vehicle's full stop at 5.5 s. Both IWMs and EWBs work together when ABS is enabled to generate a blended torque commanded by the wheel slip controller until the vehicle reaches the standstill at

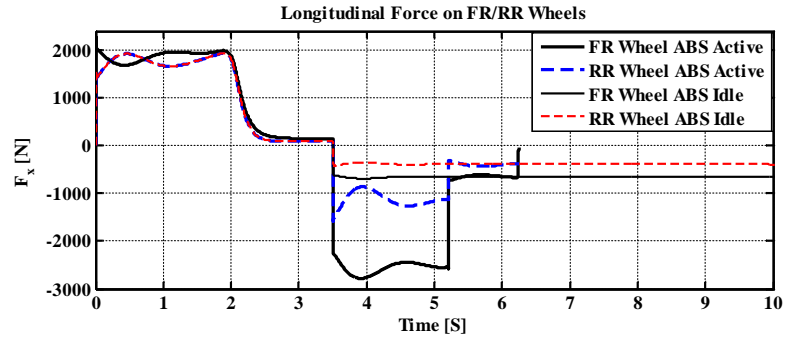


(1a)

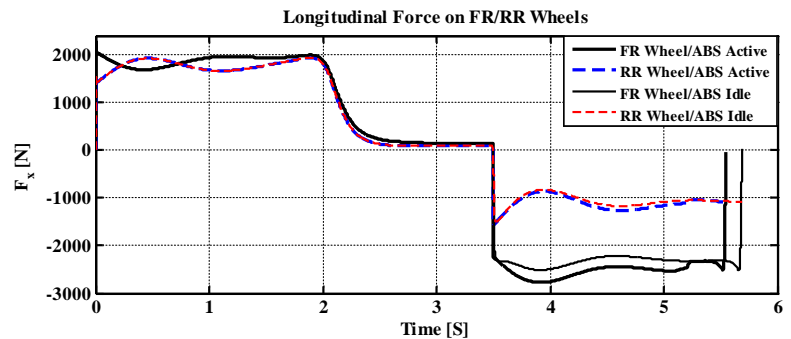


(1b)

**Figure 9.** Front (rear)-right wheels slip ratio with ABS enabled/disabled in the low-speed manoeuvre.

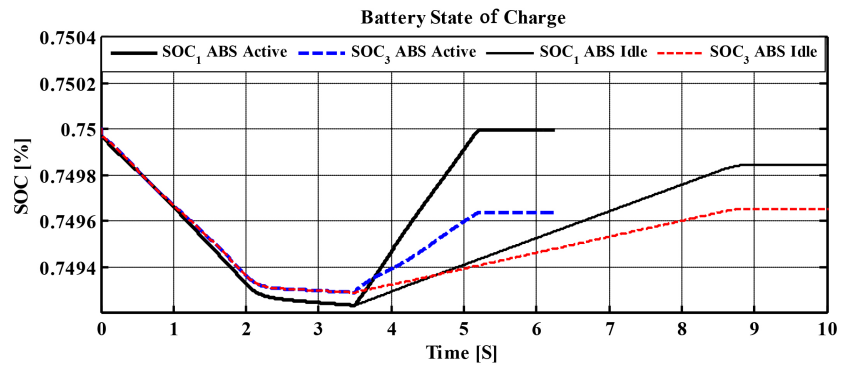


(1a)

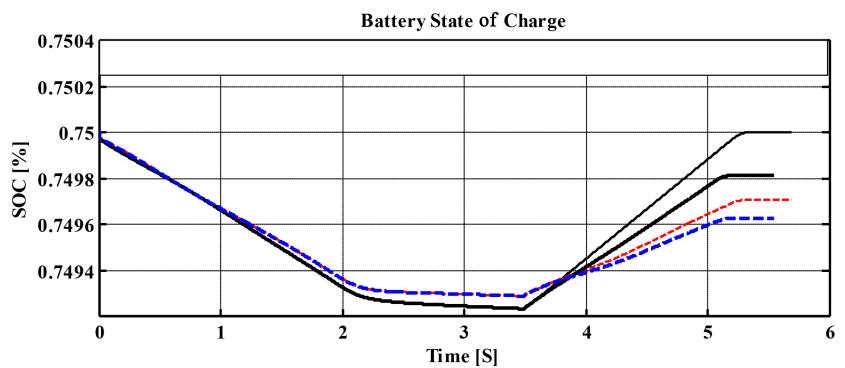


(1b)

**Figure 10.** Front (rear)-right wheels longitudinal force with ABS enabled/disabled in the low-speed manoeuvre.



(1a)



(1b)

**Figure 11.** The SOC of battery packs BP1/BP3 with ABS enabled/disabled in the low-speed manoeuvre.

5.25 s. When ABS is disabled, a blending braking mode is held, and both IWMs and EWBs collaborate to decelerate the vehicle to a complete stop at 5.7 s. **Figure 7(1b)** shows the vehicle and the front-right wheel speeds. In this scenario, there is a slight difference in vehicle stopping time (around 0.2 s) between the two modes of ABS. This difference can be related to the fact that the required torque (by wheel slip controller) is the same as the driver demand (full depression) in both cases. However, when ABS is enabled, the front-right wheel speed decreases gradually with the vehicle speed (owing to slip control). However, it drops steeply to zero after around 0.2 s from brake application with ABS disabled, indicating a locked wheel. **Figure 8(1b)** shows the regenerative and frictional torques of the front-right wheel with ABS enabled/disabled. When ABS is enabled, the IWM works below its max power providing pure regenerative torque ( $-650$  Nm), while EWB delivers the remaining portion that IWM does not cover. When ABS is disabled, the driver demands the highest braking torque where IWM works at its maximum power generating constant torque ( $-800$  Nm), and the EWB generates the top-up portion. **Figure 9(1b)** shows the slip ratio of the front (rear)-right wheels when ABS is enabled/disabled. ABS carries on wheel slip regulation at the ideal value  $\kappa \approx 0.18$ , corresponding to the highest available  $\mu_{road}$  and the highest grip force as shown in **Figure 10(1b)**. However, when ABS is disabled, the wheels' slip limit is reached, leading to a significant

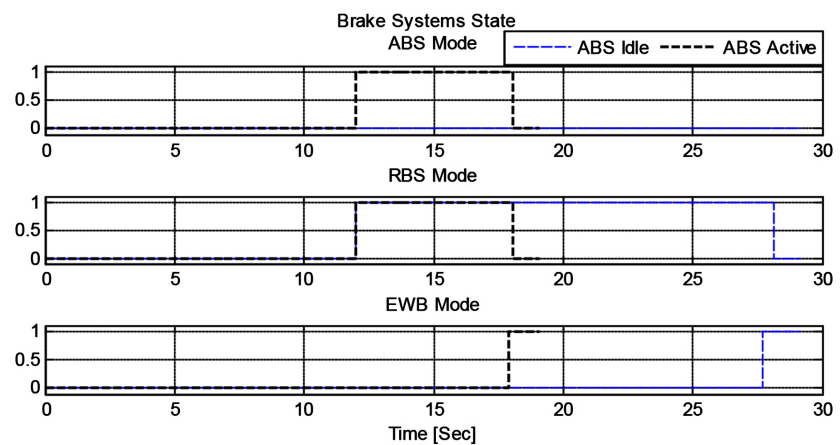
decrease in power transfer. **Figure 11(1b)** shows the SOC for battery packs BP1/BP3 when ABS is enabled/disabled. In this scenario, energy recuperation with ABS disabled is greater than that with ABS enabled. This can be explained in the same way as in the torque discussion, where maximum regenerative torque is demanded as the brake pedal is fully depressed.

## 6.2. The High-Speed Braking Manoeuvre

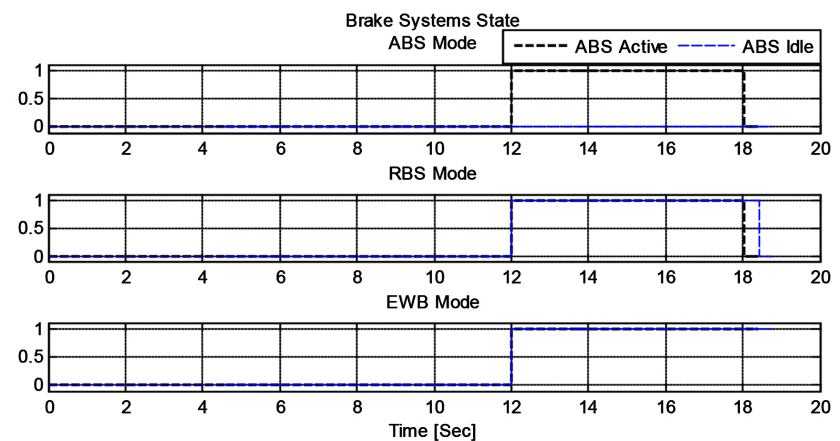
In this manoeuvre, also two braking scenarios are carried out, the regular braking with brakes partially and the emergency braking with brakes fully applied, both with the ABS enabled and disabled.

- Regular braking Scenario (2A)

For high-speed regular braking manoeuvre 2A, the same discussion of manoeuvre 1A is feasible with the only difference in initial speed and brake period. **Figure 12(2a)** showcases the operational regions of IWMs and EWBs to satisfy torque requisites during braking manoeuvre 2A under varying conditions of ABS activation. Notably, ABS becomes active upon initial brake application at 12 s,



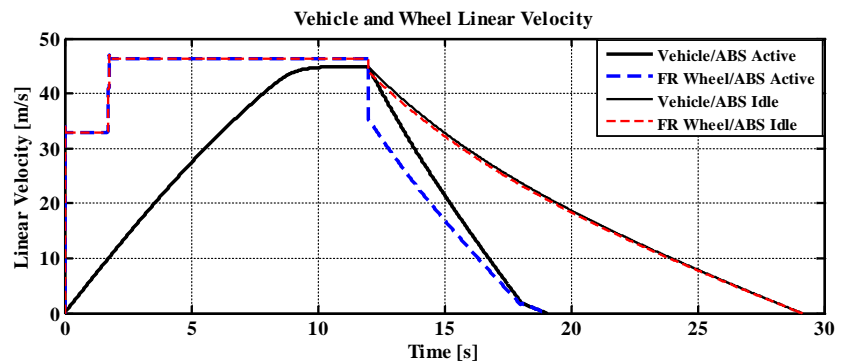
(2a)



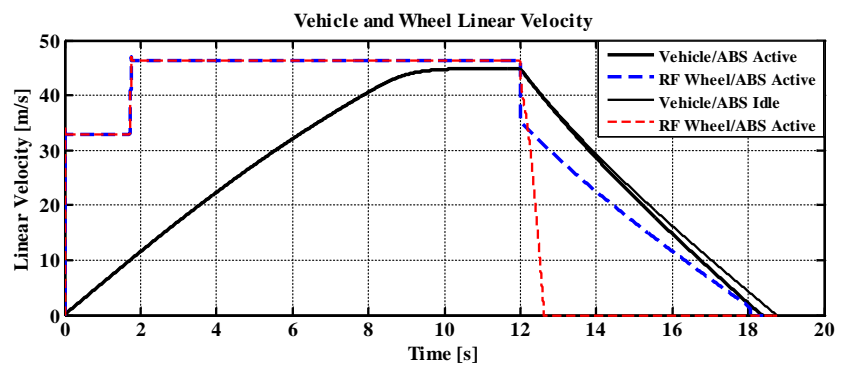
(2b)

**Figure 12.** ABS status and activation periods of IWMs and EWBs in the high-speed manoeuvre.

ceasing when the vehicle velocity drops below 7 km/h at 18 s, a point at which the control system autonomously disables ABS. When ABS is engaged, the RABS seamlessly transitions between distinct modes: commencing with the exclusive employment of pure regenerative braking (12 s - 18 s), followed by blended braking (18 s - 18.5 s), then pure frictional braking (18.5 s - 19 s) until the vehicle achieves a complete halt. Conversely, in the absence of ABS, RABS dynamically shifts between modes: initially employing pure regenerative braking (12 s - 27.6 s), subsequently transitioning to blended braking (27.6 s - 28.1 s), and ultimately resorting to pure frictional braking (28.1 s - 29 s) until the vehicle reaches a state of rest. **Figure 13(2a)** illustrates the vehicle speed and front-right wheel speed. Remarkably, the duration necessary to bring the vehicle to a complete standstill is substantially shorter (7 s) when ABS is enabled, whereas, in the absence of ABS, it is nearly 2.5 times the previous value (17 s). Thus, the implementation of ABS considerably reduces the vehicle's stopping distance. **Figure 14(2a)** elucidates the evolutions of regenerative and frictional torques exerted on the front-right wheel with and without ABS activation. Under active ABS, the IWM operates at peak capacity, supplying maximum pure regenerative torque ( $-800$  Nm) to effectuate rapid deceleration. The intervention of EWB is confined to a brief interval towards the conclusion of braking, imparting a minor braking torque. Conversely, in the idle state of ABS, the IWM generates a sustained

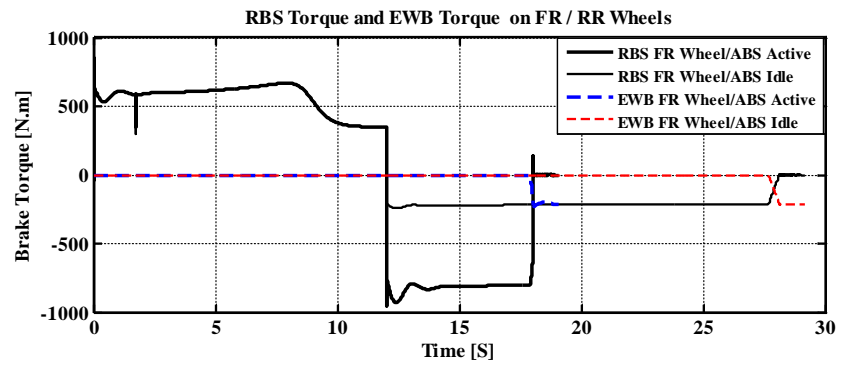


(2a)

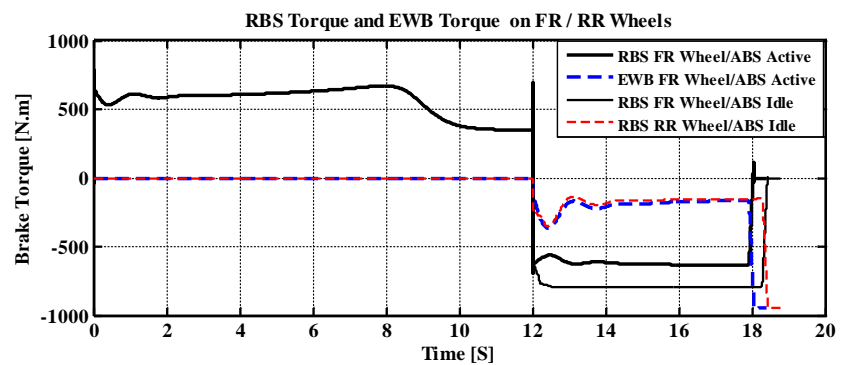


(2b)

**Figure 13.** Vehicle and front-wheel speeds with ABS enabled/disabled in the high-speed manoeuvre.



(2a)



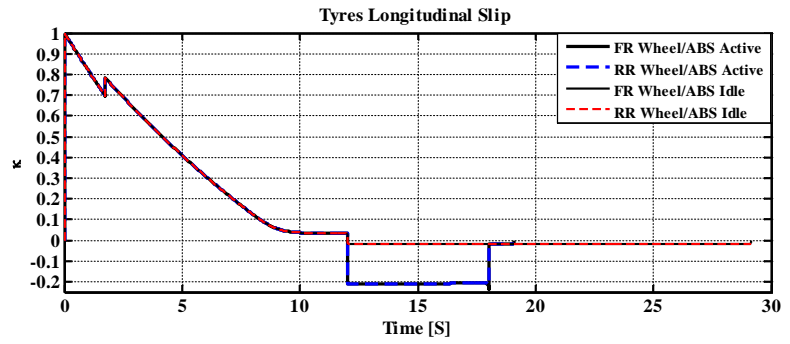
(2b)

**Figure 14.** IWM and EWB torques of the front-right wheel with ABS enabled/disabled in the high-speed manoeuvre.

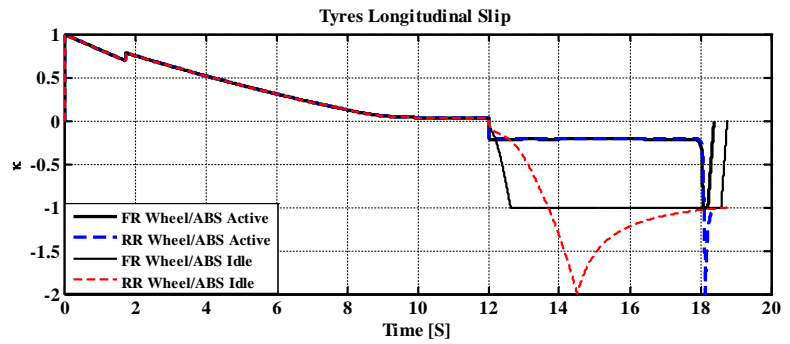
regenerative torque ( $-200$  Nm), significantly inferior to its ABS-enabled counterpart, thereby substantially elongating the stopping distance. Similarly, EWB commences its influence towards the terminal phase of braking, initially contributing a blended torque that progressively ascends until the point of IWM disengagement, subsequently persisting independently developing a pure frictional torque ( $-200$  Nm) until the vehicle attains a complete stop. **Figure 15(2a)** exhibits the slip ratio of the front (rear)-right wheels with ABS enabled/disabled. It is evident that ABS effectively regulates the slip ratio to an optimum reference value, enabling the maintenance of maximum road adhesion coefficient and hence maximum gripping force. **Figure 16(2a)** displays the brake forces exerted by the front (rear)-right wheels, indicating different ratios due to ideal distribution. **Figure 17(2a)** showcases the SOC for battery packs BP1 and BP3 when ABS is enabled or disabled. The results clearly demonstrate that ABS enhances energy recovery, leading to faster recharging of battery packs compared to when ABS is disabled.

- Emergency braking Scenario (2B)

Similarly, high-speed emergency braking manoeuvre 2B can be investigated in the same way that manoeuvres 1B is discussed with the difference in the vehicle's initial speed and brake period. **Figure 12(2b)** illustrates the operational boundaries of both IWMs and EWBs for effectively addressing the exigent braking

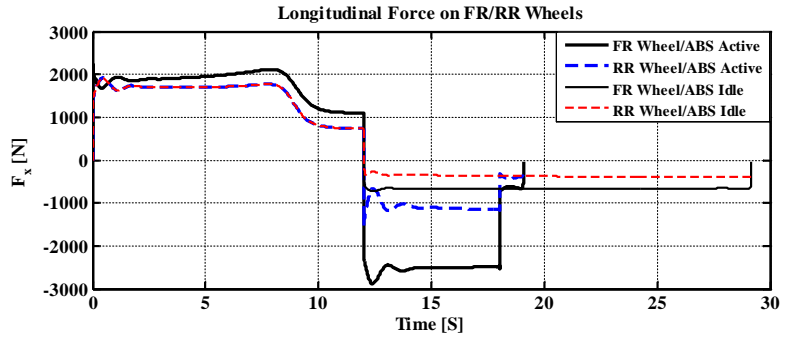


(2a)

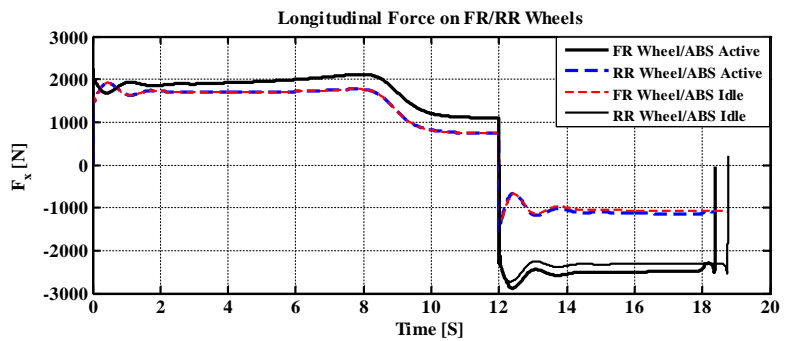


(2b)

**Figure 15.** Front (rear)-right wheels slip ratio with ABS enabled/disabled in the high-speed manoeuvre.

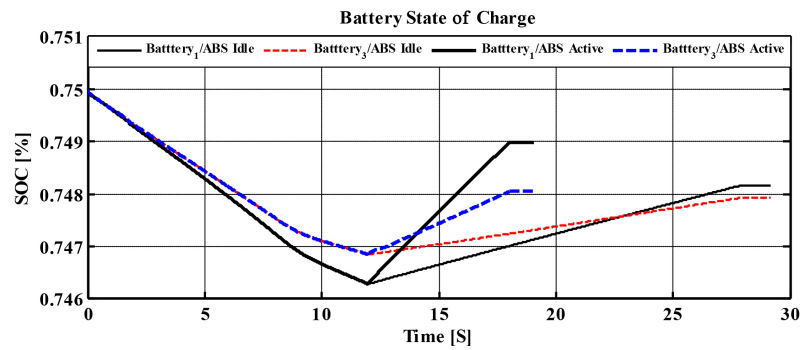


(2a)

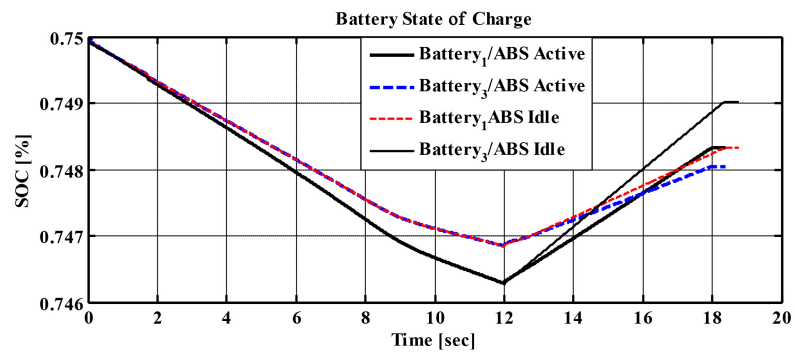


(2b)

**Figure 16.** Front (rear)-right wheels longitudinal force with ABS enabled/disabled in the high-speed manoeuvre



(2a)



(2b)

**Figure 17.** The SOC of battery packs BP1/BP3 with ABS enabled/disabled in the high-speed manoeuvre.

requirements during emergency manoeuvres with varying states of ABS activation. ABS engagement is initiated at 12 s upon brake pedal actuation and ceases when the vehicle decelerates below 7 km/h at 18 s. Subsequently, ABS is automatically disabled, enabling standard frictional braking to govern the vehicle's deceleration until it reaches a complete halt at 18.2 s. With ABS active, both IWMs and EWBs synergistically collaborate to generate a blended torque until 18 s the point at which IWMs disengage and EWBs continue delivering the remained braking torque required to bring the vehicle to a standstill at 18.2 s. Conversely, in the absence of ABS, a blending braking mode is upheld, wherein both IWMs and EWBs harmoniously cooperate producing blended braking torque over the period 12 s to 18.2 s and followed by only frictional brake by EWBs over the short final phase 18.2 s bringing the vehicle to a complete stop by 18.4 s. **Figure 13(2b)** depicts the velocity profiles of the vehicle and the front-right wheel. Within this specific context, a subtle disparity in the duration of vehicle deceleration (approximately 0.2 s) becomes evident when comparing the two ABS modes. This discrepancy can be attributed to the synchronization between the torque demanded by the wheel slip controller and the driver's full depression of the brake pedal, which remains consistent across both scenarios.

However, with ABS enabled, the front-right wheel speed experiences a gradual reduction with respect to the vehicle speed, owing to slip control mechanisms. Conversely, in the absence of ABS, the front-right wheel speed precipitously

plunges to zero within approximately 0.2 s from the initiation of brake application, indicative of wheel lockup. **Figure 14(2b)** showcases the variations of regenerative and frictional torques exerted on the front-right wheel under ABS-enabled and ABS-disabled configurations. With ABS active, the IWM operates below its peak power capacity, delivering pure regenerative torque ( $-650$  Nm), while the EWB supplies the complementary torque to compensate for the portion not covered by the IWM. In contrast, when ABS is disabled, the driver demands maximum braking torque, prompting the IWMs to operate at maximum power, providing a constant torque ( $-800$  Nm), with the EWB supplementing the residual torque requirement. **Figure 15(2b)** illustrates the wheel slip ratios observed in the front (rear)-right wheels during both ABS-enabled and ABS-disabled conditions. ABS consistently modulates the wheel slip ratio to achieve an optimal value of  $\kappa \approx 0.18$ , maintaining high adhesion with the road and, consequently, maximizing the gripping force, as validated in **Figure 16(2b)**. Conversely, when ABS is deactivated, the wheels approach their slip limits, resulting in a significant reduction in power transfer efficacy. **Figure 17(2b)** reveals the SOC profiles for battery packs BP1 and BP3 upon the activation and deactivation of ABS. In this particular configuration, energy recuperation with ABS disabled surpasses that achieved with ABS enabled. This can be explained analogously to the torque discourse, where the maximal regenerative torque is demanded in response to full depression of the brake pedal.

## 7. Conclusions

This paper proposes a coordinate wheel slip-based blended RABS control for all-IWM-drive EVs. The proposed brakes are comprised of two systems, an RBS represented in IWMs, and an FBS embodied in EWBs. The integrated functionality of both RBS and FBS can be realized as a pure BBW allowing for a proper blending of braking torque. A coordinated RABS control is suggested to manage brake torques generated by each system, ensuring maximal energy recovery and vehicle stability. The control comprises three layers: a high-level layer, an inter-layer, and a low-level layer. In the higher layer, wheels slip control takes place where the brake torque reference is calculated considering the driver's command. This reference is distributed between IWMs and EWBs in the coordinate inter-layer. In the lower layer, the control of both IWMs and EWBs is performed, where IWMs are controlled based on FOC and MTPA strategy to maximize energy recuperation, while EWBs are held with the LQR method. Based on the regenerative-frictional torque ratio, there are three modes of operation, pure regenerative braking, blended regenerative-frictional braking, and pure frictional braking. The coordinate control layer switches between the different modes according to the following:

- Pure regenerative braking

When the total brake torque demand is within the IWMs' power capacity, given that the battery SOC and the vehicle speed allow for energy recovery, IWMs are only used to generate a pure regenerative torque and energy recupera-

tion is maintained at maximum.

- Blended regenerative-frictional braking

When the required braking torque is out of the IWMs power capacity, given that the SOC state and vehicle speed factors allow for energy recovery, both IWMS and EWBs are used to generate a mixed brake torque energy recuperation is SOC-dependent.

- Pure frictional braking

When the required braking torque is within (out) the power capacity of IWMs, given that the SOC state and (or) the vehicle speed do not allow energy recovery, then EWBs are only used to generate a pure frictional braking torque, and no energy recuperation occurs.

The performance of the proposed RABS is verified through simulation tests done on a 3-DOF vehicle model with 4xIWMs and 4xEWBs in MATLAB/ Simulink with system parameters shown in **Table A1** in Appendix A. For this purpose, two straight-line braking manoeuvres were performed, the low and the high speeds, starting from 50 km/h and 150 km/h, respectively. Two scenarios are carried out in each manoeuvre: regular braking with the brake partially applied and emergency braking with the brake fully applied. The braking is conducted with the ABS enabled and disabled in each scenario. Results are demonstrated and compared in terms of vehicle speed, wheel speeds, wheel total torque, wheel slip ratio, and battery packs SOC. Simulation results of all manoeuvres showed high vehicle performance under braking with the proposed RABS control. The high performance can be Figure d out by preventing the wheels from being locked during harsh braking, ensuring maximum gripping force all the time, minimizing stopping time and distance, maximizing energy recuperation, and extending vehicle range.

## Author Contributions

The innovations and contributions of this work are summarized as follows:

- Integrated blended slip-based RABS composed of RBS (IWMs) and FBS (EWBs) for all-IWMs-drive EV is proposed
- The ability of simultaneous operation of both RBS and FBS benefiting from ABS features and regenerative braking advantages together
- Replacement of hydraulic ABS with EWB system and elimination of its disadvantages
- Realization of a full pure BBW system

The coordinate control realizes a max energy efficiency and vehicle safety at the same time.

## Conflicts of Interest

The authors declare no conflict of interest.

## Future Work

In future work, the following should be considered:

Considering vehicle safety through a fail-safe function of EWB.

Extending the simulation to include a combined wheel slip when braking at a turn and  $\mu$ -split road conditions.

## References

- [1] Wang, F., Ye, P., Xu, X., Cai, Y., Ni, S. and Que, H. (2022) Novel Regenerative Braking Method for Transient Torsional Oscillation Suppression of Planetary-Gear Electrical Powertrain. *Mechanical Systems and Signal Processing*, **163**, Article ID: 108187. <https://doi.org/10.1016/j.ymssp.2021.108187>
- [2] Gaurkar, P.V., Challa, A., Ramakrushnan, K., Subramanian, S.C., Vivekanandan, G. and Sivaram, S. (2021) Model Predictive Control of Wheel Slip towards Antilock Brake System Using Convex optimization. 2021 *International Conference on COMMunication Systems and NETWORKS*, Bangalore, 5-9 January 2021, 644-649. <https://doi.org/10.1109/COMSNETS51098.2021.9352848>
- [3] Said Jneid, M. and Harth, P. (2003) Integrated Braking and Traction Torque Vectoring Control Based on Vehicle Yaw Rate for Stability Improvement of All-Wheel-Drive Electric Vehicles. 2023 *IEEE International Conference on Electrical Systems for Aircraft, Railway, Ship Propulsion and Road Vehicles & International Transportation Electrification Conference (ESARS-ITEC)*, Venice, 29-31 March 2023, 1-6. <https://doi.org/10.1109/ESARS-ITEC57127.2023.10114899>
- [4] Said Jneid, M. and Harth, P. (2023) Integrated Torque Vectoring Control Using Vehicle Yaw Rate and Sideslip Angle for Improving Steering and Stability of All off-Wheel-Motor Drive Electric Vehicles, Forthcoming..
- [5] Joa, E., Yi, K., Sohn, K. and Bae, H. (2018) Four-Wheel Independent Brake Control to Limit Tire Slip under Unknown Road Conditions. *Control Engineering Practice*, **76**, 79-95. <https://doi.org/10.1016/j.conengprac.2018.04.001>
- [6] Hartani, K., Khalfaoui, M., Merah, A. and Aouadj, N. (2018) A Robust Wheel Slip Control Design with Radius Dynamics Observer for EV. *The SAE International Journal of Vehicle Dynamics, Stability, and NVH*, **2**, 135-146. <https://doi.org/10.4271/10-02-02-0009>
- [7] Choi, S.B. (2008) Antilock Brake System with a Continuous Wheel Slip Control to Maximize the Braking Performance and the Ride Quality. *IEEE Transactions on Control Systems Technology*, **16**, 996-1003. <https://doi.org/10.1109/TCST.2007.916308>
- [8] Montani, M., Vitaliti, D., Capitani, R. and Annicchiarico, C. (2020) Performance Review of Three Car Integrated ABS Types: Development of a Tire Independent Wheel Speed Control. *Energies*, **13**, Article 6183. <https://doi.org/10.3390/en13236183>
- [9] Challa, A., Ramakrushnan, K., Gaurkar, P.V., Subramanian, S.C., Vivekanandan, G. and Sivaram, S. (2021) A 3-Phase Combined Wheel Slip and Acceleration Threshold Algorithm for Anti-Lock Braking in Heavy Commercial Road Vehicles. *Vehicle System Dynamics*, **60**, 2312-2333. <https://doi.org/10.1080/00423114.2021.1903048>
- [10] Patil, A., Nissimagoudar, P., Naik, A., Lingadhal, A.C., Mirashi, J.V. and Ingale, K.R. (2021) Optimization of Braking-Torque in Anti-Lock Braking System Using Perturb & Observe Technique. 2021 *International Conference on Smart Generation Computing, Communication and Networking (SMART GENCON)*, Pune, 29-30 October 2021, 1-6. <https://doi.org/10.1109/SMARTGENCON51891.2021.9645850>
- [11] Harly, M. (2020) Modeling of Hydraulic ABS Plant and Its Control by Using Fuzzy

- Mamdani with Adaptive Slip Frequency to Improve Stopping Distance and Steering Ability. *Journal of Physics: Conference Series*, **1700**, Article ID: 012044. <https://doi.org/10.1088/1742-6596/1700/1/012044>
- [12] Zhang, H., Liang, H., Tao, X., Ding, Y., Yu, B. and Bai, R. (2021) Driving Force Distribution and Control for Maneuverability and Stability of a 6WD Skid-Steering EUGV with Independent Drive Motors. *Applied Sciences*, **11**, Article 961. <https://doi.org/10.3390/app11030961>
- [13] Chen, X., Wei, L., Wang, X., Li, L., Wu, Q. and Xiao, L. (2021) Hierarchical Cooperative Control of Anti-Lock Braking and Energy Regeneration for Electromechanical Brake-by-Wire System. *Mechanical Systems and Signal Processing*, **159**, Article ID: 107796. <https://doi.org/10.1016/j.ymssp.2021.107796>
- [14] Koylu, H. and Tural, E. (2021) Experimental Study on Braking and Stability Performance during Low Speed Braking with ABS under Critical Road Conditions. *Engineering Science and Technology, an International Journal*, **24**, 1224-1238. <https://doi.org/10.1016/j.jestch.2021.02.001>
- [15] You, S., Gil, J. and Kim, W. (2021) Fixed-Time Slip Control with Extended-State Observer Using Only Wheel Speed for Anti-Lock Braking Systems of Electric Vehicles. *IEEE Transactions on Intelligent Transportation Systems*, **23**, 6368-6378. <https://doi.org/10.1109/TITS.2021.3055980>
- [16] Wang, B., Huang, X., Wang, J., Guo, X. and Zhu, X. (2015) A Robust Wheel Slip Ratio Control Design Combining Hydraulic and Regenerative Braking Systems for in-Wheel-Motors-Driven Electric Vehicles. *Journal of the Franklin Institute*, **352**, 577-602. <https://doi.org/10.1016/j.jfranklin.2014.06.004>
- [17] Burton, D., Delaney, A., Newstead, S., Logan, D. and Fildes, B. (2004) Evaluation of Anti-Lock Braking Systems Effectiveness. Research Report 00/04.
- [18] Kim, J., Kwon, B., Park, Y., Cho, H.J. and Yi, K. (2021) A Control Strategy for Efficient Slip Ratio Regulation of a Pneumatic Brake System for Commercial Vehicles. *Proceedings of the Institution of Mechanical Engineers, Part D: Journal of Automobile Engineering*, 236, 1546-1567. <https://doi.org/10.1177/09544070211038466>
- [19] Yuan, Y., Zhang, J., Li, Y. and Lv, C. (2017) Regenerative Brake-by-Wire System Development and Hardware-in-Loop Test for Autonomous Electrified Vehicle. SAE Technical Papers 2017-01-0401. <https://doi.org/10.4271/2017-01-0401>
- [20] Said Jneid, M., Harth, P. and Ficzer, P. (2020) In-Wheel-Motor Electric Vehicles and Their Associated Drivetrains. *International Journal for Traffic and Transport Engineering*, **10**, 415-431. [https://doi.org/10.7708/ijtte.2020.10\(4\).01](https://doi.org/10.7708/ijtte.2020.10(4).01)
- [21] Fan, L.K., *et al.* (2022) A GA-Based Online Real-Time Optimized Energy Management Strategy for Plug-in Hybrid Electric Vehicles. *Energy*, **241**, Article ID: 122811. <https://doi.org/10.1016/j.energy.2021.122811>
- [22] Amato, G. and Marino, R. (2021) Reconfigurable Slip Vectoring Control in Four in-Wheel Drive Electric Vehicles. *Actuators*, **10**, Article 157. <https://doi.org/10.3390/act10070157>
- [23] Favilli, T., Delogu, M., Pugi, L. and Berzi, L. (2021) Functional Safety and Reliability for Innovative Vehicle Braking System and Integration with Electric Traction Units. IOP Publishing, Bristol, p. 012020.
- [24] Zhang, L., Pang, Z., Wang, S., Zhang, S. and Yuan, X. (2020) Electromechanical Composite Brake Control for Two in-Wheel Motors Drive Electric Vehicle with Single Motor Failure. *Proceedings of the Institution of Mechanical Engineers, Part D: Journal of Automobile Engineering*, **234**, 1057-1074. <https://doi.org/10.1177/0954407019864229>

- [25] Oleksowicz, S.A., *et al.* (2013) Regenerative Braking Strategies, Vehicle Safety and Stability Control Systems: Critical Use-Case Proposals. *Vehicle System Dynamics*, **51**, 684-699. <https://doi.org/10.1080/00423114.2013.767462>
- [26] Vodovozov, V., Raud, Z., Petlenkov, E. and Babu, S. (2021) Review on Braking Energy Management in Electric Vehicles. *Energies*, **14**, Article 4477. <https://doi.org/10.3390/en14154477>
- [27] Sakai, A., Miyazaki, T., Okano, T., Nimura, K. and Nakata, D. (2014) Regenerative Braking Systems. In: Crolla, D., Foster, D.G., Kobayashi, T. and Vaughan, N., Eds., *Encyclopedia of Automotive Engineering*, John Wiley & Sons, New York, 1-15. <https://doi.org/10.1002/9781118354179.auto053>
- [28] Tiwari, A. and Teja, A.V.R. (2021) Anti Lock Regenerative Braking Scheme for BLDC-Motor Driven Electric Vehicles. 2021 *IEEE 30th International Symposium on Industrial Electronics (ISIE)*, Kyoto, 20-23 June 2021, 1-6. <https://doi.org/10.1109/ISIE45552.2021.9576436>
- [29] von Albrichsfeld, C. and Karner, J. (2009) Brake System for Hybrid and Electric Vehicles. SAE Technical Paper 2009-01-1217.
- [30] Yang, C., Liu, K., Jiao, X., Wang, W., Chen, R. and You, S. (2022) An Adaptive Firework Algorithm Optimization-Based Intelligent Energy Management Strategy for Plug-in Hybrid Electric Vehicles. *Energy*, **239**, Article ID: 122120. <https://doi.org/10.1016/j.energy.2021.122120>
- [31] Zhuo, G., Yu, F. and Ren, Y. (2015) Study on the Braking Torque Allocation of the ABS Based on the Frequency of the Electro-Hydraulic Brake. SAE Technical Papers 2015-01-2703. <https://doi.org/10.4271/2015-01-2703>
- [32] Ivanov, V. and Savitski, D. (2015) Systematization of Integrated Motion Control of Ground Vehicles. *IEEE Access*, **3**, 2080-2099. <https://doi.org/10.1109/ACCESS.2015.2496108>
- [33] Zhang, J., Kong, D., Chen, L. and Chen, X. (2012) Optimization of Control Strategy for Regenerative Braking of an Electrified Bus Equipped with an Anti-Lock Braking System. *Proceedings of the Institution of Mechanical Engineers, Part D: Journal of Automobile Engineering*, **226**, 494-506. <https://doi.org/10.1177/0954407011422463>
- [34] Lv, C., Zhang, J., Li, Y. and Yuan, Y. (2015) Novel Control Algorithm of Braking Energy Regeneration System for an Electric Vehicle during Safety-Critical Driving Maneuvers. *Energy Conversion and Management*, **106**, 520-529. <https://doi.org/10.1016/j.enconman.2015.09.062>
- [35] Mei, P., Yang, S., Xu, B. and Sun, K. (2021) A Fuzzy Sliding-Mode Control for Regenerative Braking System of Electric Vehicle. 2021 *7th International Conference on Control, Automation and Robotics (ICCAR)*, Singapore, 23-26 April 2021, 397-401. <https://doi.org/10.1109/ICCAR52225.2021.9463463>
- [36] Ahangarnejad, A.H., Radmehr, A. and Ahmadian, M. (2020) A Review of Vehicle Active Safety Control Methods: From Antilock Brakes to Semiautonomy. *Journal of Vibration and Control*, **27**, 1683-1712. <https://doi.org/10.1177/1077546320948656>
- [37] Said Jneid, M., Zöldy, M. and Harth, P. (2023) Sensorless Optimal Control of Electronic Wedge Brake Based on Dynamic Model and Kalman Filter State Multiple-Estimation. *Proceedings of the Institution of Mechanical Engineers, Part D: Journal of Automobile Engineering*. <https://doi.org/10.1177/09544070231168168>
- [38] Said Jneid, M. and Joukhadar, A. (2019) LQR-Based Control of a Single Motor Electronic Wedge Brake EWB for Automotive Brake-by-Wire System. *Soft Computing and Electrical Engineering*, **1**, 12-35.
- [39] Shyrokau, B., Wang, D., Heidrich, L. and Höpping, K. (2013) Analysis of Subsystems

- Coordination for Electric Vehicle during Straight-Line Braking and Brake-in-Turn. 2013 *IEEE Symposium on Computational Intelligence for Engineering Solutions (CIES)*, Singapore, 16-19 April 2013, 61-67.
- [40] Zhang, L., Zhang, Z., Wang, Z., Deng, J. and Dorrell, D.G. (2021) Chassis Coordinated Control for Full X-by-Wire Vehicles-A Review. *Chinese Journal of Mechanical Engineering*, **34**, Article No. 42. <https://doi.org/10.1186/s10033-021-00555-6>
- [41] Jordanoska, V., Danev, D. and Changoski, V. (2021) Evaluating Coordinated Cooperative Control of Three Active Car Systems Using Fuzzy-Logic. IOP Publishing, Bristol, **1190**, p. 012029.
- [42] Aly, A.A., Zeidan, E.S., Hamed, A. and Salem, F. (2011) An Antilock-Braking Systems (ABS) Control: A Technical Review. *Intelligent Control and Automation*, **2**, 186-195. <https://doi.org/10.4236/ica.2011.23023>
- [43] Subramaniyam, K.V. and Subramanian, S.C. (2021) Electrified Vehicle Wheel Slip Control Using Responsiveness of Regenerative Braking. *IEEE Transactions on Vehicular Technology*, **70**, 3208-3217. <https://doi.org/10.1109/TVT.2021.3066095>
- [44] Tang, Q., Yang, Y., Luo, C., Yang, Z. and Fu, C. (2022) A Novel Electro-Hydraulic Compound Braking System Coordinated Control Strategy for a Four-Wheel-Drive Pure Electric Vehicle Driven by Dual Motors. *Energy*, **241**, Article ID: 122750. <https://doi.org/10.1016/j.energy.2021.122750>
- [45] Zhao, W., Wu, G., Wang, C., Yu, L. and Li, Y. (2019) Energy Transfer and Utilization Efficiency of Regenerative Braking with Hybrid Energy Storage System. *Journal of Power Sources*, **427**, 174-183. <https://doi.org/10.1016/j.jpowsour.2019.04.083>
- [46] Mei, P., Karimi, H.R., Yang, S., Xu, B. and Huang, C. (2021) An Adaptive Fuzzy Sliding-Mode Control for Regenerative Braking System of Electric Vehicles. *Journal of Adaptive Control and Signal Processing*, **36**, 391-410. <https://doi.org/10.1002/acs.3347>
- [47] Vodovozov, V., Aksjonov, A., Petlenkov, E., Raud, Z. and Romero-Cadaval, E. (2021) Neural Network-Based Model Reference Control of Braking Electric Vehicles. *Energies*, **14**, Article 2373. <https://doi.org/10.3390/en14092373>
- [48] Torinsson, J., Jonasson, M., Yang, D. and Jacobson, B. (2020) Energy Reduction by Power Loss Minimisation through Wheel Torque Allocation in Electric Vehicles: A Simulation-Based Approach. *Vehicle System Dynamics*, **60**, 1488-1511. <https://doi.org/10.1080/00423114.2020.1858121>
- [49] Heydrich, M., *et al.* (2021) Integrated Braking Control for Electric Vehicles with in-Wheel Propulsion and Fully Decoupled Brake-by-Wire System. *Vehicles*, **3**, 145-161. <https://doi.org/10.3390/vehicles3020009>
- [50] De Castro, R., Araújo, R.E., Tanelli, M., Savaresi, S.M. and Freitas, D. (2012) Torque blending and Wheel Slip Control in EVs with in-Wheel Motors. *Vehicle System Dynamics*, **50**, 71-94. <https://doi.org/10.1080/00423114.2012.666357>
- [51] Han, J. and Park, Y. (2014) Cooperative Regenerative Braking Control for Front-Wheel-Drive Hybrid Electric Vehicle Based on Adaptive Regenerative Brake Torque Optimization Using Under-Steer Index. *International Journal of Automotive Technology*, **15**, 989-1000. <https://doi.org/10.1007/s12239-014-0104-9>
- [52] Ding, S., Liu, L. and Zheng, W.X. (2017) Sliding Mode Direct Yaw-Moment Control Design for in-Wheel Electric Vehicles. *IEEE Transactions on Industrial Electronics*, **64**, 6752-6762. <https://doi.org/10.1109/TIE.2017.2682024>
- [53] Pacejka, H.B. (2012) *Tire and Vehicle Dynamics*. Butterworth-Heinemann, Oxford.
- [54] Nam, K. (2015) *Application of Novel Lateral Tire Force Sensors to Vehicle Parame-*

- ter Estimation of Electric Vehicles. *Sensors*, **15**, 28385-28401. <https://doi.org/10.3390/s151128385>
- [55] Bisht, V., Saravanakumar, D., Sakthivel, G. and Sivakumar, R. (2021) Yaw Moment Compensation by Actuator-Based Control of Brake System in Automobiles. *Journal of Physics: Conference Series*, **1969**, Article ID: 012063.
- [56] Su, L., Wang, Z. and Chen, C. (2022) Torque Vectoring Control System for Distributed Drive Electric Bus under Complicated Driving Conditions. *Assembly Automation*, **42**, 1-18. <https://doi.org/10.1108/AA-12-2020-0194>
- [57] Miranda, M.H.R., Silva, F.L., Lourenço, M.A.M., Eckert, J.J. and Silva, L.C.A. (2022) Electric Vehicle Powertrain and Fuzzy Controller Optimization Using a Planar Dynamics Simulation Based on a Real-World Driving Cycle. *Energy*, **238**, Article ID: 121979. <https://doi.org/10.1016/j.energy.2021.121979>
- [58] Boerboom, M. (2012) Electric Vehicle Blended Braking Maximizing Energy Recovery While Maintaining Vehicle Stability and Manouverability. Master's Thesis, Chalmers University of Technology, Göteborg.
- [59] Yeo, H., Koo, C., Jung, W., Kim, D. and Cheon, J.S. (2011) Development of Smart Booster Brake Systems for Regenerative Brake Cooperative Control. SAE Technical Paper 2011-01-2356. <https://doi.org/10.4271/2011-01-2356>
- [60] Yin, G., Wang, S. and Jin, X. (2013) Optimal Slip Ratio Based Fuzzy Control of Acceleration Slip Regulation for Four-Wheel Independent Driving Electric Vehicles. *Mathematical Problems in Engineering*, **2013**, Article ID: 410864. <https://doi.org/10.1155/2013/410864>
- [61] Singh, K.B., Arat, M.A. and Taheri, S. (2013) An Intelligent Tire Based Tire-Road Friction Estimation Technique and Adaptive Wheel Slip Controller for Antilock Brake System. *The Journal of Dynamic Systems, Measurement, and Control*, **135**, Article ID: 031002. <https://doi.org/10.1115/1.4007704>
- [62] Qiu, Y., Liang, X. and Dai, Z. (2015) Backstepping Dynamic Surface Control for an Anti-Skid Braking System. *Control Engineering Practice*, **42**, 140-152. <https://doi.org/10.1016/j.conengprac.2015.05.013>
- [63] Reif, K. (2014) Brakes, Brake Control and Driver Assistance Systems Function, Regulation and Components Bosch Professional Automotive Information. Springer, Berlin.
- [64] Boisvert, M. and Micheau, P. (2016) Estimators of Wheel Slip for Electric vehicles Using Torque and Encoder Measurements. *Mechanical Systems and Signal Processing*, **76-77**, 665-676. <https://doi.org/10.1016/j.ymssp.2016.02.017>
- [65] Mirzaeinejad, H. and Mirzaei, M. (2010) A Novel Method for Non-Linear Control of Wheel Slip in Anti-Lock Braking Systems. *Control Engineering Practice*, **18**, 918-926. <https://doi.org/10.1016/j.conengprac.2010.03.015>
- [66] Chowdhri, N., Ferranti, L., Iribarren, F.S. and Shyrokau, B. (2021) Integrated Non-Linear Model Predictive Control for Automated Driving. *Control Engineering Practice*, **106**, Article ID: 104654. <https://doi.org/10.1016/j.conengprac.2020.104654>

## Appendix

**Table A1.** Systems parameters.

Related System	Parameter	Related System	Parameter		
	<b>EWB</b>		<b>Vehicle</b>		
<b>Wedge</b>	$\alpha$	0.342°	$M_v$	1250 kg	
	$\beta$	0.342°	$A_f$	2.17 m <sup>2</sup>	
	$\mu_p$	0.352	$C_d$	0.3	
	$M_w$	0.7 Kg	$L_f$	1.07 m	
	$K_{cal}$	$1.2 \times 10^8$ N/m	$L_r$	1.605 m	
	$\eta$	0.85	$T_{wf}$	1.517 m	
<b>Screw Axle</b>	$K_A$	$8 \times 10^8$ N/m	$T_{wr}$	1.505 m	
	$D_A$	$1 \times 10^4$ Nm·s/rad	$h_{CG}$	0.543 m	
	$L$	$0.5 \times 10^{-3}$ m	$I_x$	540 kg·m <sup>2</sup>	
	$R_M$	11.8 $\Omega$	$I_y$	2398 kg·m <sup>2</sup>	
<b>DC Motor</b>	$L_M$	0.2 H	$I_z$	2617 kg·m <sup>2</sup>	
	$J_M$	$6.8 \times 10^{-3}$ Kg·m <sup>2</sup>	$g$	9.81 m/s <sup>2</sup>	
	$D_M$	$5.74 \times 10^{-4}$ Nm·s/rad	$I_T$	1 kg·m <sup>2</sup>	
	$U_M$	220 V	$T_M$	1.558 Nm	
	$I_M$	1.64 A	<b>Tire</b>	$r_e$	0.316 m
	$\omega_M$	209 rad/s	$R_e$	0.2 m	
	$T_M$	1.558 Nm	$\mu_{road}$	0.8	
	$K_e \cdot \varphi$	0.949			
	$K_t \cdot \varphi$	0.949			
	<b>Protean Motor Parameters</b>				
<b>IWM</b>	$L_d = L_q$	1.89 mH			
	$R_s$	0.16 $\Omega$			
	$\Phi_f$	0.068 Web			
	$P$	64			
	$F$	0.0064 Nm·s/rad			
	$J$	0.0389 Kg·m <sup>2</sup>			
	$\omega_b$	1000 rpm			
	$I_n$	30 A			
	$V_n$	380 V			
$T_{cm}$	500 Nm				